An Improved Control Method for Standalone Brushless Doubly-Fed Induction Generator Under Unbalanced and Nonlinear Loads Using Dual-Resonant Controller

Mohammed, Omer Mohammed Elbabo; Xu, Wei; Liu, Yi; Blaabjerg, Frede

Published in:
I E E E Transactions on Industrial Electronics

DOI (link to publication from Publisher):
10.1109/TIE.2020.2994891

Publication date:
2021

Document Version
Accepted author manuscript, peer reviewed version

An Improved Control Method for Standalone Brushless Doubly-Fed Induction Generator Under Unbalanced and Nonlinear Loads Using Dual-Resonant Controller

Omer Mohammed Elbabo Mohammed, Wei Xu, *Senior Member*, *IEEE*, Yi Liu, *Member*, *IEEE*, and Frede Blaabjerg, *Fellow*, *IEEE*

Abstract—The brushless doubly-fed induction generator (BDFIG) in standalone mode is sensitive to unusual working situations, particularly unbalanced and nonlinear loads. The unbalanced and nonlinear loads can cause significant unbalance and distortion for voltage and current of the power winding (PW). In PW voltage under nonlinear and unbalanced loads, the component of negative sequence represents the unbalance influence, and the 5th and 7th harmonics components represent the nonlinear influence. To address these issues, the dual-resonant controller (DRC) is employed to reduce the unbalance and nonlinear influences of PW voltage via generating the reference command of control winding (CW) voltage which compensate the negative sequence component and 5th and 7th harmonic components of PW voltage through the machine side converter (MSC). The experimental and simulation tests are applied to check the effectiveness of the proposed strategy.

***Index Terms*— Brushless doubly-fed induction generator (BDFIG), dual-resonant controller (DRC), nonlinear load, standalone operation, unbalanced load.**

NOMENCLATURE

ω	Angular speed.
p	Pole pair.
i, u, φ	Current, voltage and flux vectors.
L, R, M	Self-inductance, resistance, and mutual inductance.
s	Differential operator.
F	General electrical vector representing voltage, flux, or current vector.
Subscripts	
c, p, r	Control winding, power winding, and rotor.
+, -	Positive and negative sequences.
3, 5, 7	3rd, 5th, and 7th harmonic components.
Superscripts	
+, -	Positive and negative frames.
3, 5, 7	3rd, 5th, and 7th harmonic frames.

This work was supported in part by the National Natural Science Foundation of China under Grants 51707079 and 51877093, the National Key Research and Development Program of China under Grant YS2018YFGH000299, the Key Technical Innovation Program of Hubei Province under Grant 2019AAA026. (Corresponding author: Wei Xu).

O. M. Elbabo Mohammed is with the State Key Laboratory of Advanced Electromagnetic Engineering and Technology, School of Electrical and Electronic Engineering, Huazhong University of Science and Technology, Wuhan 430074, China, and also with the Department of Electrical Engineering, Faculty of Engineering, University of Sinnar, Sinnar 11174, Sudan (e-mail: babo271@yahoo.com)

W. Xu and Y. Liu are with the State Key Laboratory of Advanced Electromagnetic Engineering and Technology, School of Electrical and Electronic Engineering, Huazhong University of Science and Technology, Wuhan, 430074, China (e-mail: weixu@hust.edu.cn; liuyi82@hust.edu.cn).

F. Blaabjerg is with the Department of Energy Technology, Aalborg University, DK-9220 Aalborg, Denmark (e-mail: fbl@et.aau.dk).

I. Introduction

The brushless double-fed induction generator (BDFIG) is expected to be one of leading machines in the coming years for standalone generation mode, this is due to the particular design structure without brushes and slip rings that make the machine more durable and reliable [1], [2]. The three different parts which are called stator power winding (PW), stator control winding (CW) and the distinguishing rotor are represented the main composition of BDFIG [3], [4]. Fig. 1 depicts the simplified scheme of BDFIG in standalone mode.

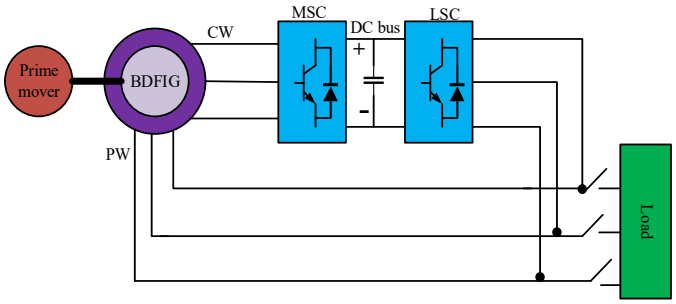

Fig. 1. Simplified scheme of BDFIG in standalone mode.

In the grid mode, control strategies aim to guarantee the generation of active and reactive power under usual or unusual working situations [1]-[6]. And, in the standalone mode, control strategies aim to guarantee stability of magnitude and frequency of PW voltage under usual [7]-[10] or unusual working situations [14]-[17]. Under usual circumstances, a scalar control has been presented in [7], the feature of which is the low implementation cost. For vessels generator systems, authors in

[8] adopted three various controllers to set the amplitude and frequency of PW voltage and the amplitude of CW current. In [9], numerical frequency domain controller has been adopted to avoid the complicated aberrations to obtain more accurate design consequences of BDFIG. For developing inner current loops in BDFIG, decoupling network has been presented without the rotor position data, which can decrease the number of sensors and consequently reduce the cost of the system [10].

There are many unusual operating situations which occur with the BDFIG. This paper focuses on two unusual situations which would occur when the BDFIG works under unbalanced and nonlinear loads in the standalone mode. Under the unbalanced load, the negative sequence component exists in the system, and the PW voltage becomes unbalanced. Under the nonlinear load, the PW voltage becomes distorted, containing odd harmonic components with frequencies of 6n±1 (n=1, 2,...) multiples of the PW frequency. Either of nonlinear or unbalanced loads lead to deteriorating the connected normal loads, which can cause failure of electrical devices. As a result, the BDFIG stator windings may be exposed to internal heating, high current, and torque pulsation, which may decrease the lifetime of BDFIG [11]-[13].

In [14], for vessels generator systems, the compensator of PW voltage has been adopted to address unbalance case in PW voltage. The compensator of PW voltage can generate three-phase CW voltage in negative frame to minimize the unbalanced influence of PW voltage. The drawback of this method is the tendency to use many feedback quantities as well as many filters. As a result, the system becomes expensive and difficult to implement. In [15], the compensator of negative sequence voltage has been developed to address unbalance influence in PW voltage. The compensator of negative sequence voltage can output CW current commands in positive frame and negative sequence. The drawback of this strategy is the need to use the filter to extract the negative sequence component of PW voltage. In [16], the sensorless phase control has been proposed to reduce the unbalance of PW voltage, the major drawback of which is that an additional loop is used to adjust the phase angle, and consequently raises prospect of fault in compensation operation.

Under nonlinear loads, the past literatures on BDFIG focus on the compensation for two significance values (i.e. odd harmonic 5th and 7th components). In [17], The coordinated compensation method through MSC and load-side converter (LSC) has been presented. The weight factor is adopted to realize the distributing contribution of harmonics compensation between MSC and LSC at the same time. The drawback of this strategy is the need of a filter to extract the 5th and 7th harmonic components. The design of the compensation method becomes more complicated due to the dependence on two converters to achieve the process of compensation.

From aforementioned literatures, we can find that the common feature of all the compensation methods is the dependence on filters to extract the negative sequence component or 5th and 7th harmonic components, whether under unbalanced load or nonlinear load. Unfortunately, this may decrease the system response time, and increases P, PI or PIR controllers to complete the compensation process. In addition, the design methodology would be more complex and the system cost becomes very high.

To overcome the aforementioned issues, this paper proposes the dual-resonant controller (DRC) in MSC to achieve compensation when the system is under nonlinear or unbalanced loads. The DRC composes of two resonant controllers which are called the unbalance resonant controller and the harmonics resonant controller, respectively. The advantages of applying DRC in the standalone BDFIG can be briefly summarized as follows:

1) The filters to extract the negative sequence component or 5th and 7th harmonic components can be removed. The numbers of PIR, P and PI controllers can be significantly reduced, leading to improve the system response.
2) The design methodology of the DRC is easier and the computational burden can be decreased.
3) The ability of working under unbalanced or nonlinear loads can be achieved.

II. Performance Analysis of BDFIG Under Unbalanced and Nonlinear Loads

The speed of rotor of BDFIG can be clarified as

$$\omega_r = (\omega_p + \omega_c)/(p_p + p_c)\ . \tag{1}$$

In the normal condition, the BDFIG mathematical model can be expressed as [18]

$$u_p = R_p i_p + s\varphi_p + j\omega_p \varphi_p \tag{2}$$

$$u_c = R_c i_c + s\varphi_c - j\omega_c \varphi_c \tag{3}$$

$$u_r = R_r i_r + s\varphi_r + j(\omega_p - p_p \omega_r)\varphi_r \tag{4}$$

$$\varphi_p = L_p i_p + M_{pr} i_r \tag{5}$$

$$\varphi_c = L_c i_c + M_{cr} i_r \tag{6}$$

$$\varphi_r = L_r i_r + M_{pr} i_p + M_{cr} i_c\ . \tag{7}$$

A. Analysis Under Unbalanced Load

Under the unbalanced load, the current, flux and voltage vectors can be split into the negative and positive components as follows:

$$F^+ = \underbrace{F_+^+}_{\text{postive component}} + \underbrace{F_-^+}_{\text{negative component}} = \underbrace{F_+^+}_{\text{postive component}} + \underbrace{F_-^- e^{-j2\omega_p t}}_{\text{negative component}}\ . \tag{8}$$

From (8), the flux, voltage and current vectors of PW in the positive fundamental frame can be derived as

$$\begin{cases} u_p^+ = u_{p+}^+ + u_{p-}^- e^{-j2\omega_p t} \\ i_p^+ = i_{p+}^+ + i_{p-}^- e^{-j2\omega_p t} \\ \varphi_p^+ = \varphi_{p+}^+ + \varphi_{p-}^- e^{-j2\omega_p t} \end{cases}\ . \tag{9}$$

Substituting (9) into (2) and (5), PW negative and positive sequences voltage equations in identical reference frames can be expressed as

$$u_{p+}^+ = R_p i_{p+}^+ + s\varphi_{p+}^+ + j\omega_p \varphi_{p+}^+ \tag{10}$$

$$u_{p-}^- = R_p i_{p-}^- + s\varphi_{p-}^- - j\omega_p \varphi_{p-}^-\ . \tag{11}$$

By using the same method, the PW negative and positive sequences flux equations can be acquired by

$$\varphi_{p+}^{+} = L_p i_{p+}^{+} + M_{pr} i_{r+}^{+} \tag{12}$$

$$\varphi_{p-}^{-} = L_p i_{p-}^{-} + M_{pr} i_{r-}^{-}. \tag{13}$$

The same procedure is used to acquire the negative and positive sequence flux and voltage equations of rotor and CW. Thus, under unbalanced loads, the BDFIG model can be divided into two combinations of equations as follows:

$$\begin{cases} u_{p+}^{+} = R_p i_{p+}^{+} + s\varphi_{p+}^{+} + j\omega_p \varphi_{p+}^{+} \\ \varphi_{p+}^{+} = L_p i_{p+}^{+} + M_{pr} i_{r+}^{+} \\ u_{c+}^{+} = R_c i_{c+}^{+} + s\varphi_{c+}^{+} + j(\omega_p - (p_p + p_c)\omega_r)\varphi_{c+}^{+} \\ \varphi_{c+}^{+} = L_c i_{c+}^{+} + M_{cr} i_{r+}^{+} \\ u_{r+}^{+} = R_r i_{r+}^{+} + s\varphi_{r+}^{+} + j(\omega_p - p_p\omega_r)\varphi_{r+}^{+} \\ \varphi_{r+}^{+} = L_r i_{r+}^{+} + M_{pr} i_{p+}^{+} + M_{cr} i_{c+}^{+} \end{cases} \tag{14}$$

$$\begin{cases} u_{p-}^{-} = R_p i_{p-}^{-} + s\varphi_{p-}^{-} - j\omega_p \varphi_{p-}^{-} \\ \varphi_{p-}^{-} = L_p i_{p-}^{-} + M_{pr} i_{r-}^{-} \\ u_{c-}^{-} = R_c i_{c-}^{-} + s\varphi_{c-}^{-} + j(-\omega_p - (p_p + p_c)\omega_r)\varphi_{c-}^{-} \\ \varphi_{c-}^{-} = L_c i_{c-}^{-} + M_{cr} i_{r-}^{-} \\ u_{r-}^{-} = R_r i_{r-}^{-} + s\varphi_{r-}^{-} + j(-\omega_p - p_p\omega_r)\varphi_{r-}^{-} \\ \varphi_{r-}^{-} = L_r i_{r-}^{-} + M_{pr} i_{p-}^{-} + M_{cr} i_{c-}^{-} \end{cases} \tag{15}$$

where (14) and (15) represent the mathematical equations of the positive and negative components, respectively.

B. Analysis Under Three-Phase Nonlinear Load

Under the three-phase nonlinear load, the current, flux and voltage can be split into the harmonics and positive fundamental component as follow [19]

$$\begin{aligned} F^{+} &= \underbrace{F_{+}^{+}}_{\text{postive component}} + \underbrace{F_{5}^{+}}_{5^{th}\text{ component}} + \underbrace{F_{7}^{+}}_{7^{th}\text{ component}} \\ &= \underbrace{F_{+}^{+}}_{\text{postive component}} + \underbrace{F_{5}^{5} e^{-j6\omega_p t}}_{5^{th}\text{ component}} + \underbrace{F_{7}^{7} e^{j6\omega_p t}}_{7^{th}\text{ component}}. \end{aligned} \tag{16}$$

To obtain the mathematical equations of the BDFIG under nonlinear load, similar procedure, which is applied under unbalanced load analysis is adopted to derive the positive, 5th, and 7th components for flux and voltage equations of the rotor, PW and CW. Thus, under the three-phase nonlinear load, the BDFIG model can be divided into three sets of equations as follows:

$$\begin{cases} u_{p+}^{+} = R_p i_{p+}^{+} + s\varphi_{p+}^{+} + j\omega_p \varphi_{p+}^{+} \\ \varphi_{p+}^{+} = L_p i_{p+}^{+} + M_{pr} i_{r+}^{+} \\ u_{c+}^{+} = R_c i_{c+}^{+} + s\varphi_{c+}^{+} + j(\omega_p - (p_p + p_c)\omega_r)\varphi_{c+}^{+} \\ \varphi_{c+}^{+} = L_c i_{c+}^{+} + M_{cr} i_{r+}^{+} \\ u_{r+}^{+} = R_r i_{r+}^{+} + s\varphi_{r+}^{+} + j(\omega_p - p_p\omega_r)\varphi_{r+}^{+} \\ \varphi_{r+}^{+} = L_r i_{r+}^{+} + M_{pr} i_{p+}^{+} + M_{cr} i_{c+}^{+} \end{cases} \tag{17}$$

$$\begin{cases} u_{p5}^{5} = R_p i_{p5}^{5} + s\varphi_{p5}^{5} + j(-5)\omega_p \varphi_{p5}^{5} \\ \varphi_{p5}^{5} = L_p i_{p5}^{5} + M_{pr} i_{r5}^{5} \\ u_{c5}^{5} = R_c i_{c5}^{5} + s\varphi_{c5}^{5} + j(-5\omega_p - (p_p + p_c)\omega_r)\varphi_{c5}^{5} \\ \varphi_{c5}^{5} = L_c i_{c5}^{5} + M_{cr} i_{r5}^{5} \\ u_{r5}^{5} = R_r i_{r5}^{5} + s\varphi_{r5}^{5} + j(-5\omega_p - p_p\omega_r)\varphi_{r5}^{5} \\ \varphi_{r5}^{5} = L_r i_{r5}^{5} + M_{pr} i_{p5}^{5} + M_{cr} i_{c5}^{5} \end{cases} \tag{18}$$

$$\begin{cases} u_{p7}^{7} = R_p i_{p7}^{7} + s\varphi_{p7}^{7} + j7\omega_p \varphi_{p7}^{7} \\ \varphi_{p7}^{7} = L_p i_{p7}^{7} + M_{pr} i_{r7}^{7} \\ u_{c7}^{7} = R_c i_{c7}^{7} + s\varphi_{c7}^{7} + j(7\omega_p - (p_p + p_c)\omega_r)\varphi_{c7}^{7} \\ \varphi_{c7}^{7} = L_c i_{c7}^{7} + M_{cr} i_{r7}^{7} \\ u_{r7}^{7} = R_r i_{r7}^{7} + s\varphi_{r7}^{7} + j(7\omega_p - p_p\omega_r)\varphi_{r7}^{7} \\ \varphi_{r7}^{7} = L_r i_{r7}^{7} + M_{pr} i_{p7}^{7} + M_{cr} i_{c7}^{7} \end{cases} \tag{19}$$

where (17), (18) and (19) represent the mathematical equations of the positive, 5th harmonic, and 7th harmonic components, respectively.

C. Analysis Under Single-Phase Nonlinear Load

Under the single-phase nonlinear load, the most significant harmonics include the negative fundamental and positive third harmonics [20], [21]. Thus, the current, flux and voltage can be split into the third harmonic, the negative, and positive fundamental components as follows:

$$\begin{aligned} F^{+} &= \underbrace{F_{+}^{+}}_{\text{postive component}} + \underbrace{F_{-}^{+}}_{\text{negative component}} + \underbrace{F_{3}^{+}}_{3^{th}\text{ component}} \\ &= \underbrace{F_{+}^{+}}_{\text{postive component}} + \underbrace{F_{-}^{-} e^{-2j\omega_p t}}_{\text{negative component}} + \underbrace{F_{3}^{3} e^{2j\omega_p t}}_{3^{th}\text{ component}}. \end{aligned} \tag{20}$$

From (20), the voltage, current, and flux vectors of PW in the positive reference frame can be expressed as

$$\begin{cases} u_p^{+} = u_{p+}^{+} + u_{p-}^{-} e^{-j2\omega_p t} + u_{p3}^{3} e^{j2\omega_p t} \\ i_p^{+} = i_{p+}^{+} + i_{p-}^{-} e^{-j2\omega_p t} + i_{p3}^{3} e^{j2\omega_p t} \\ \varphi_p^{+} = \varphi_{p+}^{+} + \varphi_{p-}^{-} e^{-j2\omega_p t} + \varphi_{p3}^{3} e^{j2\omega_p t} \end{cases}. \tag{21}$$

By substituting (21) into (2) and (5), the PW positive, negative, and third harmonic voltage equations in the corresponding reference frames can be derived as

$$u_{p+}^{+} = R_p i_{p+}^{+} + s\varphi_{p+}^{+} + j\omega_p \varphi_{p+}^{+} \tag{22}$$

$$u_{p-}^{-} = R_p i_{p-}^{-} + s\varphi_{p-}^{-} - j\omega_p \varphi_{p-}^{-} \tag{23}$$

$$u_{p3}^{3} = R_p i_{p3}^{3} + s\varphi_{p3}^{3} + j3\omega_p \varphi_{p3}^{3}. \tag{24}$$

Similarly, the PW positive, negative, and third harmonic flux equations can be obtained by

$$\varphi_{p+}^{+} = L_p i_{p+}^{+} + M_{pr} i_{r+}^{+} \tag{25}$$

$$\varphi_{p-}^{-} = L_p i_{p-}^{-} + M_{pr} i_{r-}^{-} \tag{26}$$

$$\varphi_{p3}^{3} = L_p i_{p3}^{3} + M_{pr} i_{r3}^{3}. \tag{27}$$

A similar procedure can also be employed to derive the positive fundamental, negative fundamental and third harmonic voltage and flux equations of the CW and rotor. Thus, under single-phase non-linear load, the BDFIG model can be divided into three sets of equations as follows:

$$\begin{cases} u_{p+}^{+} = R_p i_{p+}^{+} + s\varphi_{p+}^{+} + j\omega_p \varphi_{p+}^{+} \\ \varphi_{p+}^{+} = L_p i_{p+}^{+} + M_{pr} i_{r+}^{+} \\ u_{c+}^{+} = R_c i_{c+}^{+} + s\varphi_{c+}^{+} + j(\omega_p - (p_p + p_c)\omega_r)\varphi_{c+}^{+} \\ \varphi_{c+}^{+} = L_c i_{c+}^{+} + M_{cr} i_{r+}^{+} \\ u_{r+}^{+} = R_r i_{r+}^{+} + s\varphi_{r+}^{+} + j(\omega_p - P_p \omega_r)\varphi_{r+}^{+} \\ \varphi_{r+}^{+} = L_r i_{r+}^{+} + M_{pr} i_{p+}^{+} + M_{cr} i_{c+}^{+} \end{cases} \tag{28}$$

$$\begin{cases} u_{p-}^{-} = R_p i_{p-}^{-} + s\varphi_{p-}^{-} - j\omega_p \varphi_{p-}^{-} \\ \varphi_{p-}^{-} = L_p i_{p-}^{-} + M_{pr} i_{r-}^{-} \\ u_{c-}^{-} = R_c i_{c-}^{-} + s\varphi_{c-}^{-} + j(-\omega_p - (p_p + p_c)\omega_r)\varphi_{c-}^{-} \\ \varphi_{c-}^{-} = L_c i_{c-}^{-} + M_{cr} i_{r-}^{-} \\ u_{r-}^{-} = R_r i_{r-}^{-} + s\varphi_{r-}^{-} + j(-\omega_p - P_p \omega_r)\varphi_{r-}^{-} \\ \varphi_{r-}^{-} = L_r i_{r-}^{-} + M_{pr} i_{p-}^{-} + M_{cr} i_{c-}^{-} \end{cases} \tag{29}$$

$$\begin{cases} u_{p3}^{3} = R_p i_{p3}^{3} + s\varphi_{p3}^{3} + j3\omega_p \varphi_{p3}^{3} \\ \varphi_{p3}^{3} = L_p i_{p3}^{3} + M_{pr} i_{r3}^{3} \\ u_{c3}^{3} = R_c i_{c3}^{3} + s\varphi_{c3}^{3} + j(3\omega_p - (p_p + p_c)\omega_r)\varphi_{c3}^{3} \\ \varphi_{c3}^{3} = L_c i_{c3}^{3} + M_{cr} i_{r3}^{3} \\ u_{r3}^{3} = R_r i_{r3}^{3} + s\varphi_{r3}^{3} + j(3\omega_p - p_p \omega_r)\varphi_{r3}^{3} \\ \varphi_{r3}^{3} = L_r i_{r3}^{3} + M_{pr} i_{p3}^{3} + M_{cr} i_{c3}^{3} \end{cases} \tag{30}$$

where (28), (29), and (30) represent the mathematical equations of the positive fundamental, negative fundamental, and 3rd harmonic components, respectively.

III. Conventional Control Method

All conventional methods applied in the standalone mode focuses on treating the stability of PW voltage under the change of speed or load. The direct voltage control (DVC) as shown in Fig. 2 represents one of the most common methods in the standalone mode. The DVC is realized via setting i_{cq}^{*} to zero. Therefore, the i_{cd}^{*} is equal to the CW current amplitude. Therefore, the PW voltage amplitude is adjusted via CW current i_{cd}. The actual PW voltage amplitude $|U_p|$ can be given by

$$|U_p| = \sqrt{u_{pd}^2 + u_{pq}^2}. \tag{31}$$

To keep the PW voltage frequency at 50 Hz, the frequency of the CW should be varied immediately when the rotor speed varies [22].

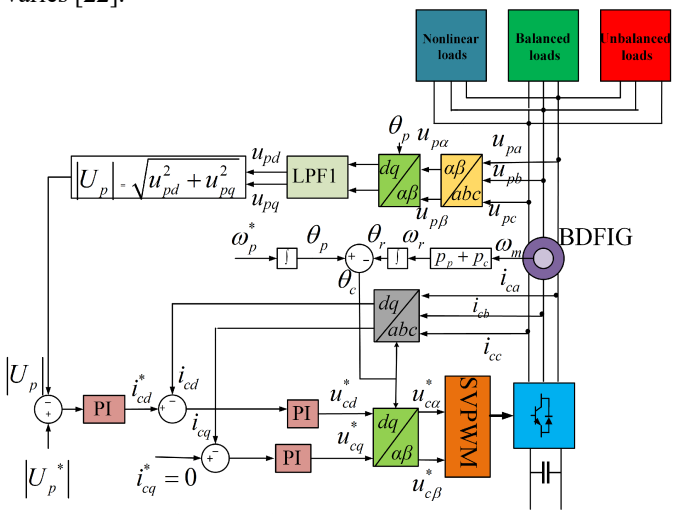

Fig. 2. Conventional control scheme [20].

IV. Proposed Control Method

The concept of the proposed methodology depends on the relation between the voltages of PW and CW derived from the BDFIG model as follow.

In steady state, the differential terms are equal to zero, and the PW and CW voltage equations in (2) and (3) can be simplified to

$$u_p = R_p i_p + j\omega_p \varphi_p \tag{32}$$

$$u_c = R_c i_c - j\omega_c \varphi_c. \tag{33}$$

Then, rearranging (32) and (5), the new expressions of PW flux and rotor current can be derived as

$$\varphi_p = (u_p - R_p i_p)/j\omega_p \tag{34}$$

$$i_r = (\varphi_p - L_p i_p)/M_{pr}. \tag{35}$$

Substituting (34) into (35), the rotor current can be given by

$$i_r = \frac{(u_p - R_p i_p)/(j\omega_p) - L_p i_p}{M_{pr}}. \tag{36}$$

Substituting (36) into (6), the CW flux can be obtained as

$$\varphi_c = L_c i_c + M_{cr}\frac{(u_p - R_p i_p)/(j\omega_p) - L_p i_p}{M_{pr}}. \quad (37)$$

Substituting (37) into (33), the relation between CW voltage and PW voltage can be expressed as

$$u_c = R_c i_c - j\omega_c\left(L_c i_c + M_{cr}\frac{(u_p - R_p i_p)/(j\omega_p) - L_p i_p}{M_{pr}}\right). \quad (38)$$

Hence, by neglecting the voltages drop of PW and CW, Eq. (38) becomes

$$u_c = -j\omega_c(M_{cr}u_p / j\omega_p M_{pr}). \quad (39)$$

From (39), the relation is linear between PW voltage and CW voltage. As a result, by adopting the similar mathematical steps introduced in (32)-(39), the comprehensive equations for a linear relation between the PW voltage and CW voltage under unbalanced load, three phase nonlinear load, and single phase nonlinear load can be obtained as follows:

$$\begin{aligned} u_c + u_{c-}^{-} &= \underbrace{-j\omega_c(M_{cr}u_p / j\omega_p M_{pr})}_{\text{Postive Component}} \\ &\underbrace{+j(-\omega_p - (p_p + p_c)\omega_r)(M_{cr}u_{p-}^{-} / -j\omega_p M_{pr})}_{\text{Negative Component}} \end{aligned} \quad (40)$$

$$\begin{aligned} u_c + u_{c5}^{5} + u_{c7}^{7} &= \underbrace{-j\omega_c(M_{cr}u_p / j\omega_p M_{pr})}_{\text{Fundamental Component}} \\ &\underbrace{+j(-5\omega_p - (p_p + p_c)\omega_r)(M_{cr}u_{p5}^{5} / j(-5)\omega_p M_{pr})}_{\text{Fifth Component}} \\ &\underbrace{+j(7\omega_p - (p_p + p_c)\omega_r)(M_{cr}u_{p7}^{7} / j7\omega_p M_{pr})}_{\text{Seventh Component}} \end{aligned} \quad (41)$$

$$\begin{aligned} u_c + u_{c-}^{-} + u_{c3}^{3} &= \underbrace{-j\omega_c(M_{cr}u_p / j\omega_p M_{pr})}_{\textit{postive component}} \\ &\underbrace{+j(-\omega_p - (p_p + p_c)\omega_r)(M_{cr}u_{p-}^{-} / -j\omega_p M_{pr})}_{\textit{negative component}} \\ &\underbrace{+j(3\omega_p - (p_p + p_c)\omega_r)(M_{cr}u_{p3}^{3} / j3\omega_p M_{pr})}_{3^{rd}\ \textit{component}} \end{aligned} \quad (42)$$

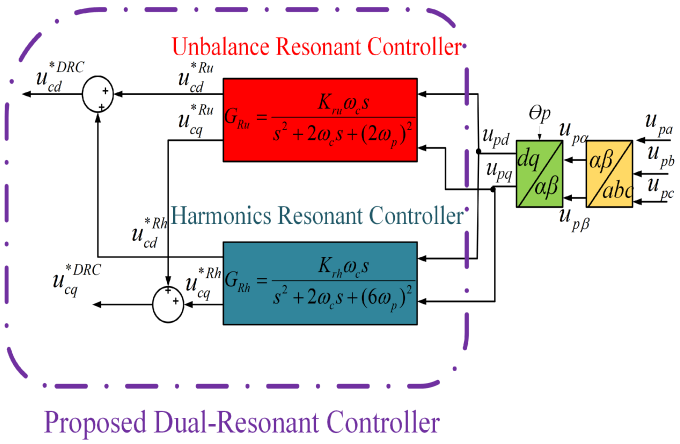

Fig. 3. Block diagram of the dual-resonant controller.

Through this concept, the dual- resonant controller (DRC) shown in Fig. 3 is proposed to reduce the nonlinear and unbalance influences of PW voltage by generating the reference command of the CW voltage, which compensates the negative component, 3rd, 5th, and 7th harmonics through the machine side converter (MSC).

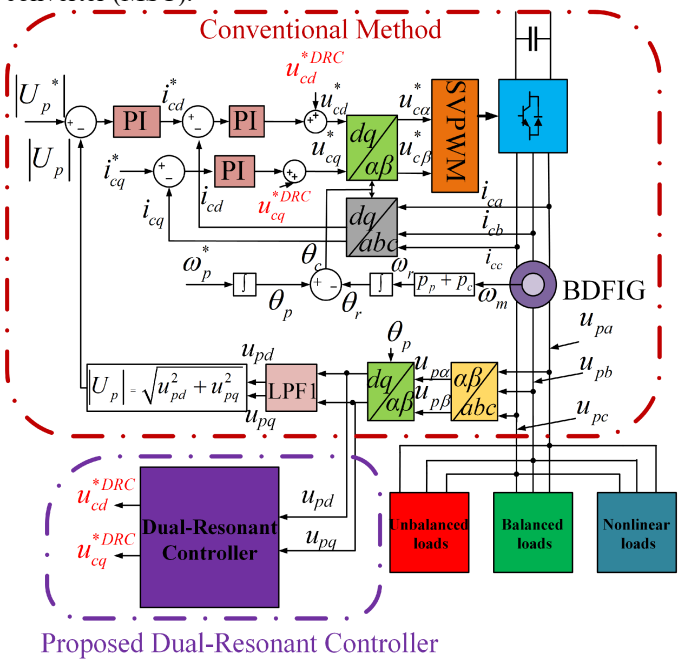

Fig. 4. Overall control scheme.

The DRC composes of two parts: unbalance resonant controller and the harmonics resonant controller. The unbalance resonant controller is responsible for compensating the unbalanced effect and third harmonic effect in PW voltage, which can be achieved by extracting the negative sequence component of PW voltage through setting the resonant frequency as $2\omega_p$ and tuning appropriate cut-off frequency ω_c and resonant gain K_{ru} to generating the new reference command of the CW voltage.

The transfer function of the unbalance resonant controller can be expressed as

$$G_{Ru} = \frac{K_{ru}\omega_c s}{s^2 + 2\omega_c s + (2\omega_p)^2} \quad (43)$$

where K_{ru} is the unbalance resonant gain.

The harmonics resonant controller is required for minimizing the nonlinear influence in PW voltage, which can be carried out by extracting the 5th and 7th harmonics of PW voltage through choosing the resonant frequency as $6\omega_p$ and setting suitable cut-off frequency ω_c and resonant gain K_{rh} to creating the new reference command of the CW voltage. The transfer function of the harmonics resonant controller can be clarified as

$$G_{Rh} = \frac{K_{rh}\omega_c s}{s^2 + 2\omega_c s + (6\omega_p)^2} \quad (44)$$

where K_{rh} is the harmonics resonant gain.

From (43) and (44), the transfer function of DRC can be given by

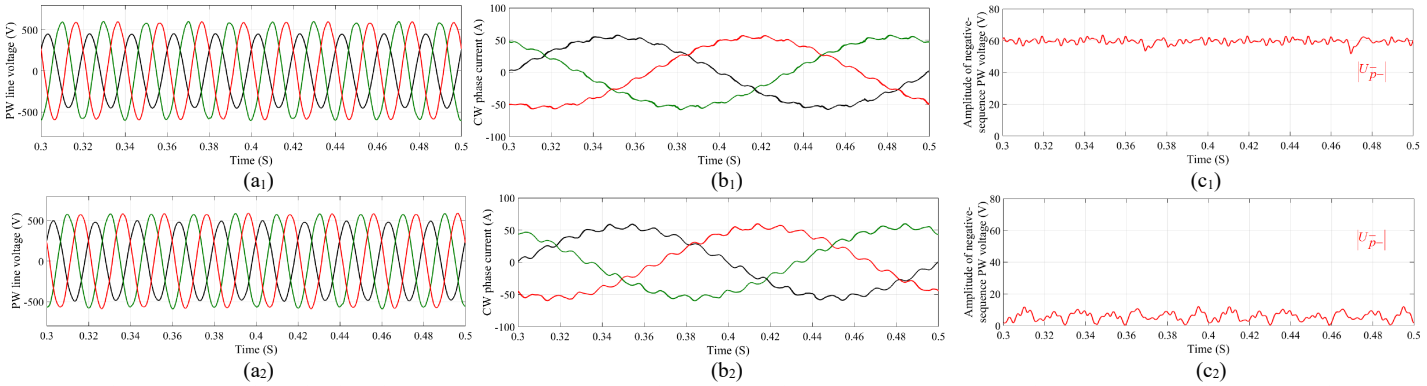

Fig. 5. Simulation results with single-phase load at 675 rpm (subscripts 1and 2 represents the conventional and proposed strategy respectively). (a) PW voltage. (b) CW current. (c) PW voltage amplitude in negative sequence.

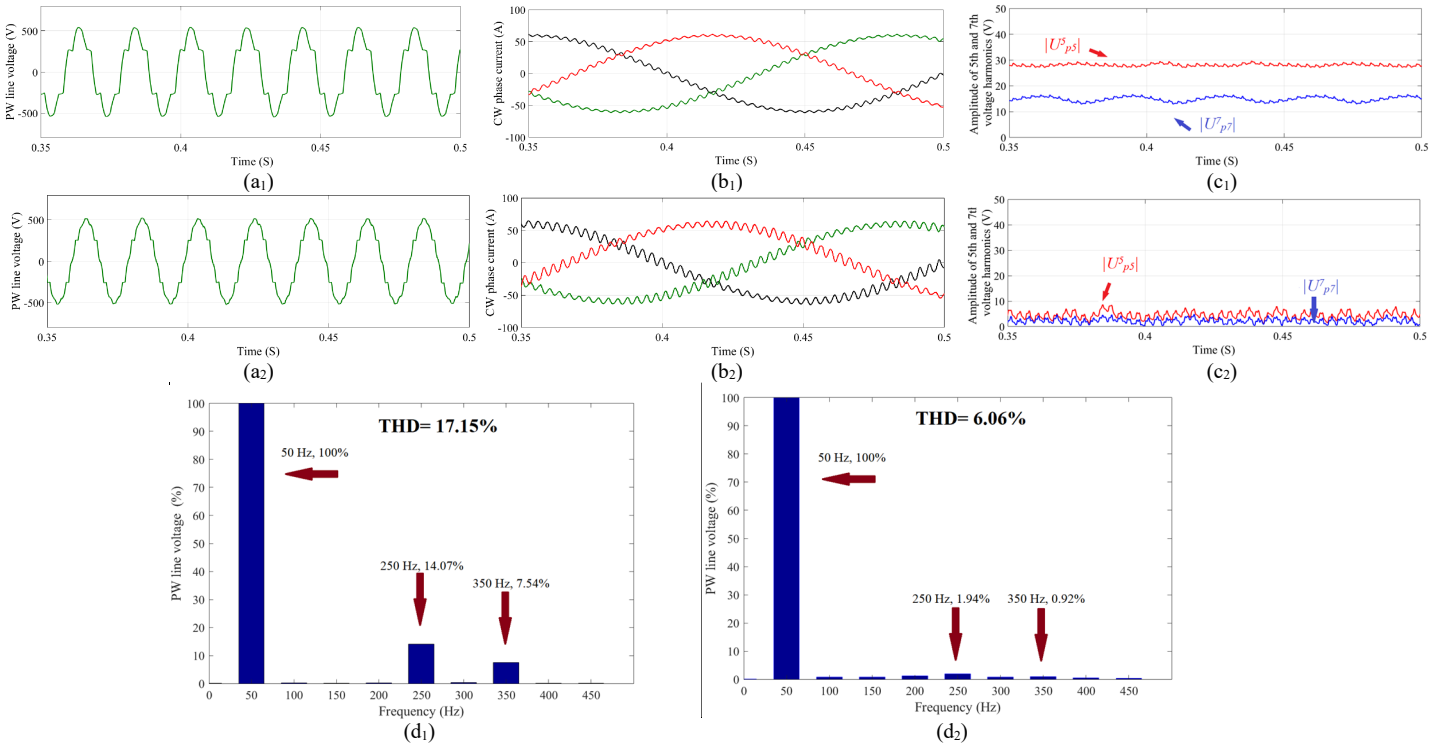

Fig. 6. Simulation results with nonlinear load at 675 rpm (subscripts 1and 2 represents the conventional and proposed strategy respectively). (a) PW voltage. (b) CW current. (c) PW phase voltage amplitude of the 5th and 7th harmonics. (d) THD of PW voltage.

$$G_{DRC} = \frac{K_{ru}\omega_c s}{s^2 + 2\omega_c s + (2\omega_p)^2} + \frac{K_{rh}\omega_c s}{s^2 + 2\omega_c s + (6\omega_p)^2} \quad . \qquad (45)$$

Fig. 4 depicts the overall control scheme with DRC in the system.

V. Simulation Results

The MATLAB/Simulink program is adopted for simulation of the proposal controller. For the unbalanced situation, the resistance of 12 Ω which is linked between phases *b* and *c* is adopted to achieve a single-phase load. This type of load provides a significantly unbalanced influence in the system.

For the nonlinear case, the nonlinear load is a diode bridge with a resistor of 25 Ω in the dc side, this value of the resistor in the dc side gives a high effect of nonlinear in PW voltage. Consequently, when minimizing the undesirable effects of PW voltage, this gives much confidence of the proposed method. Table I shows the list of parameters details which is used in the platform. A constant speed of 675 rpm is adopted for all tests.

Firstly, under unbalanced situation, Fig. 5. shows the comparison between the conventional control strategy and proposed control strategy. The conventional strategy fails to address the unbalanced influence in the PW voltage. Thus, the amount of PW voltage amplitude in the negative sequence reach an average value of around 60 V, which can be calculated by

$$\left|U_{p-}^{-}\right| = \sqrt{(u_{pd-}^{-})^2 + (u_{pq-}^{-})^2} \quad . \qquad (46)$$

The proposed method succeeds to reduce the unbalanced influence in PW voltage. Therefore, the PW voltage amplitude in the negative sequence is significantly reduced to an average value 10 V. As a result, the distortion of CW current with proposed strategy becomes larger than that with the conventional strategy.

Secondly, under nonlinear situation, Fig. 6 illustrates a comparison of the results between the proposed strategy and the conventional strategy. The conventional strategy cannot treat the nonlinear effect in the PW voltage. Thus, the amount of the amplitudes of the PW voltage in 5th and 7th harmonics are increased to 29 V and 17 V, respectively, which can be obtained as

$$\left|U_{p5}^{5}\right| = \sqrt{(u_{pd5}^{5})^2 + (u_{pq5}^{5})^2} \,. \tag{47}$$

$$\left|U_{p7}^{7}\right| = \sqrt{(u_{pd7}^{7})^2 + (u_{pq7}^{7})^2} \,. \tag{48}$$

The proposed method succeeds to minimize the nonlinear effect in the PW voltage. Therefore, the PW voltage amplitudes in 5th and 7th harmonics are significantly decreased and reach an average value of 3 V and 2 V, respectively. Consequently, the distortion of the CW current with the proposed strategy is severer than that with the conventional strategy. Figs. 6(d1) and (d2) show the total harmonic distortion (THD) of the PW voltage. With the conventional strategy, the THD reaches 17.15%. Fortunately, it can be decereased to 6.06% with the proposed strategy.

The third simulation is carried out to check the dynamic performance of the proposed method under the variable speed from the sub- to super-synchronous speed. The corresponding simulation results are shown in Fig.7. The BDFIG is started under the three-phase unbalanced and nonlinear loads and at the sub-synchronous speed of 675 rpm with the proposed method. To evaluate the dynamic performance, the rotor accelerates from sub-synchronous speed 675 rpm at 0.2 s to super-synchronous speed 875 rpm at 0.7 s. As it can be seen from Fig.7, the proposed control method maintains the balanced and linear PW voltage during the speed variation.

TABLE I
PARAMETERS OF BDFIG

PARAMETER	VALUE	PARAMETER	VALUE
Rotor type	Wound rotor	Speed range	600 ~1200 rpm
L_p	0.47492 H	PW rated voltage	380 V
L_c	0.032156 H	PW rated current	45 A
L_r	0.22523 H	PW pole pairs	1
L_{pr}	0.30685 H	CW pole pairs	3
M_{cr}	0.025840 H	CW voltage range	0~350 V
R_c	0.26803 Ω	CW current range	0~60 A
R_p	0.40335 Ω	Capacity	30 kVA
R_r	0.33385 Ω		

VI. EXPERIMENTAL RESULTS

A. Experimental Setup

The experimental setup, which is shown in Fig.8, includes four main parts; a 30 kVA BDFIG, a three-phase 37 kW induction motor, back-to-back converter, and load box.

For unbalanced situation, the resistor of 12 Ω is linked between phases b and c to achieve a single-phase load; this type of load provides a great amount of unbalanced influence in the system. For the nonlinear case, the resistor of 25 Ω connected with a diode bridge is adopted to achieve a three phase nonlinear load.

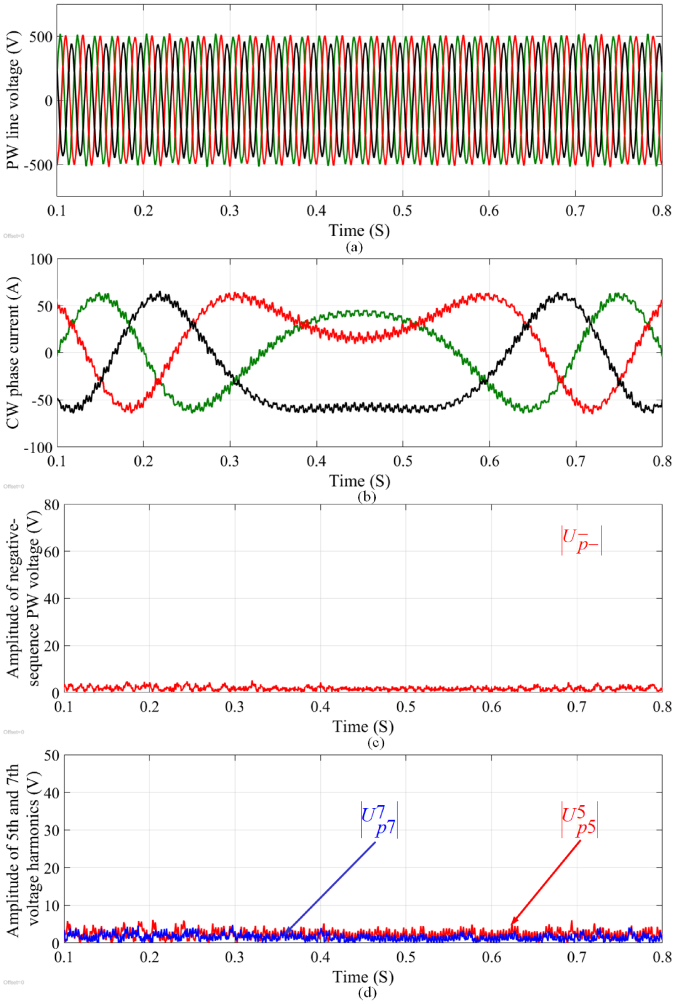

Fig. 7. Simulation results with a three-phase unbalanced and nonlinear loads under the variable rotor speed. (a) PW line voltage. (b) CW phase current. (c) PW voltage amplitude in negative sequence. (d) PW voltage amplitude of 5th and 7th harmonics.

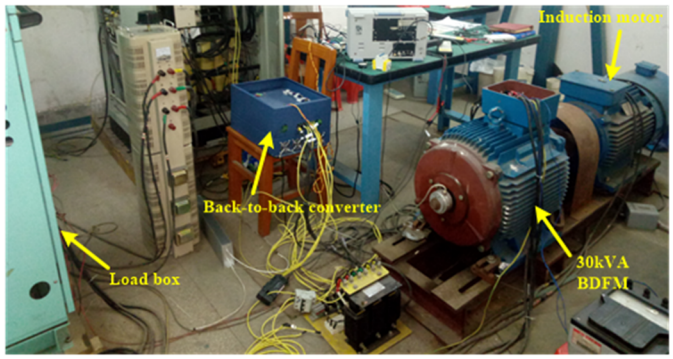

Fig. 8. Photograph of the experimental test platform.

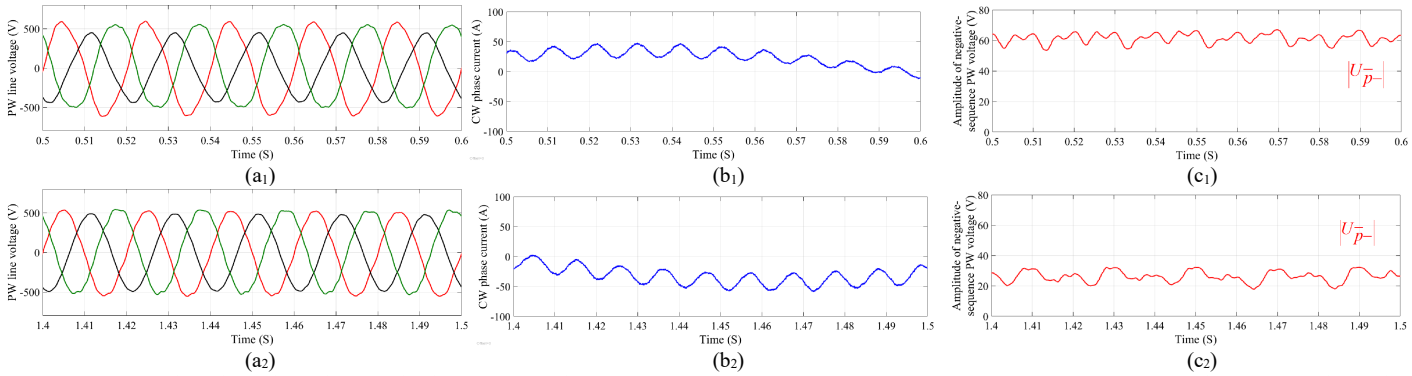

Fig. 9. Experimental results with single-phase load at 675 rpm (subscripts 1and 2 represent the conventional and proposed strategy respectively). (a) PW voltage. (b) CW current. (c) PW voltage amplitude in negative sequence.

For unbalanced and nonlinear loads, the unbalanced load is a three-phase unbalanced load (25 Ω, 50 Ω, and 50 Ω in the three phases), and the nonlinear load is a diode bridge with a resistor of 25 Ω in the dc side.

For unbalanced nonlinear load, this situation is realized via adopting a single-phase diode rectifier with a resistor of 25 Ω in the dc side. Table I shows the list of parameter details, which are used in the platform. The constant speed of 675 rpm is adopted for all tests.

B. Results Under Unbalanced Loads

Under the unbalanced case, Fig. 9. presents results of the proposed method, which are similar to simulation results presented in Fig. 5. This indicates the effectiveness of the proposed method.

Fig. 10 shows another test that is adopted to check the dynamic performance of the proposed strategy. The BDFIG starts with the conventional strategy, and it fails to address the unbalanced influence in the PW voltage.

Thus, the amount of PW voltage amplitude in the negative sequence can reach an average value of 60 V. At 1.16 s, the proposed DRC strategy is activated in the system. PW voltage amplitude in negative sequence is significantly reduced from 60 V to 22 V within 0.05 s. Thus, the unbalance influence of PW voltage is greatly minimized with good dynamic performance of the DRC.

C. Results Under Three Phase Nonlinear Loads

Under the nonlinear situation, Fig. 11. demonstrates experimental results of the proposed method, which are similar to simulations as shown in Fig. 6. This presents the effectiveness of the proposed method.

Fig. 12 illustrates another experiment used to test the dynamic operation of proposed method. The BDFIG begins with the conventional strategy. Consequently, the amount of the amplitudes of the PW voltage in 5^{th} and 7^{th} harmonics are increased to the average values of 32 V and 17 V, respectively. At 0.7 s, the proposed DRC strategy is started in the system. The amplitudes of PW voltage in 5^{th} and 7^{th} harmonics are significantly decreased from 32 V and 17 V to 7 V within 0.2 s. Thus, the nonlinear effect of the PW voltage can be significantly decreased and achieved with good dynamic operation of the DRC.

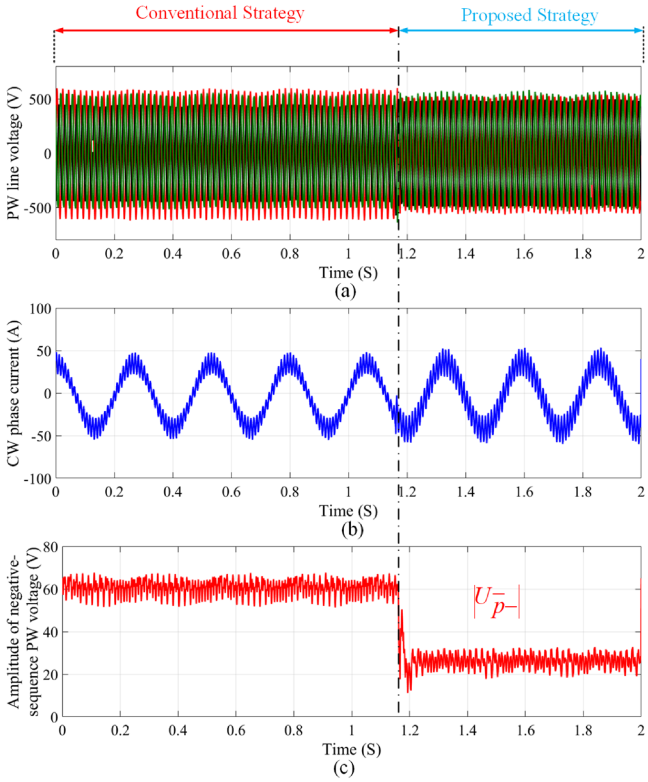

Fig. 10. Experimental dynamic performance test with the single-phase load at 675 rpm. (a) PW voltage. (b) CW current. (c) PW voltage amplitude in negative sequence.

D. Results Under Unbalanced and Nonlinear Loads

Both unbalanced and nonlinear loads are applied at the same time. The unbalanced load is a three-phase unbalanced load (25 Ω, 50 Ω, and 50 Ω in the three phases), and the nonlinear load is a diode bridge with a resistor of 25 Ω in the dc side with the reference value of PW voltage 173V. From Fig. 13, the BDFIG works under unbalanced and nonlinear loads at the same time. The BDFIG starts to work with the conventional strategy. As a result, both the unbalance effect and nonlinear effect exist in PW voltage, which is very clear in Fig. 13(d). The THD of PW voltage reaches 12.12% as shown in Fig. 13(f), and the amplitude of negative sequence component reaches around 17 V. At 3.7 s, the proposed method is activated. As a result, both undesirable effects of PW voltage are reduced as shown in Fig. 13(e), which makes the PW voltage more balanced and

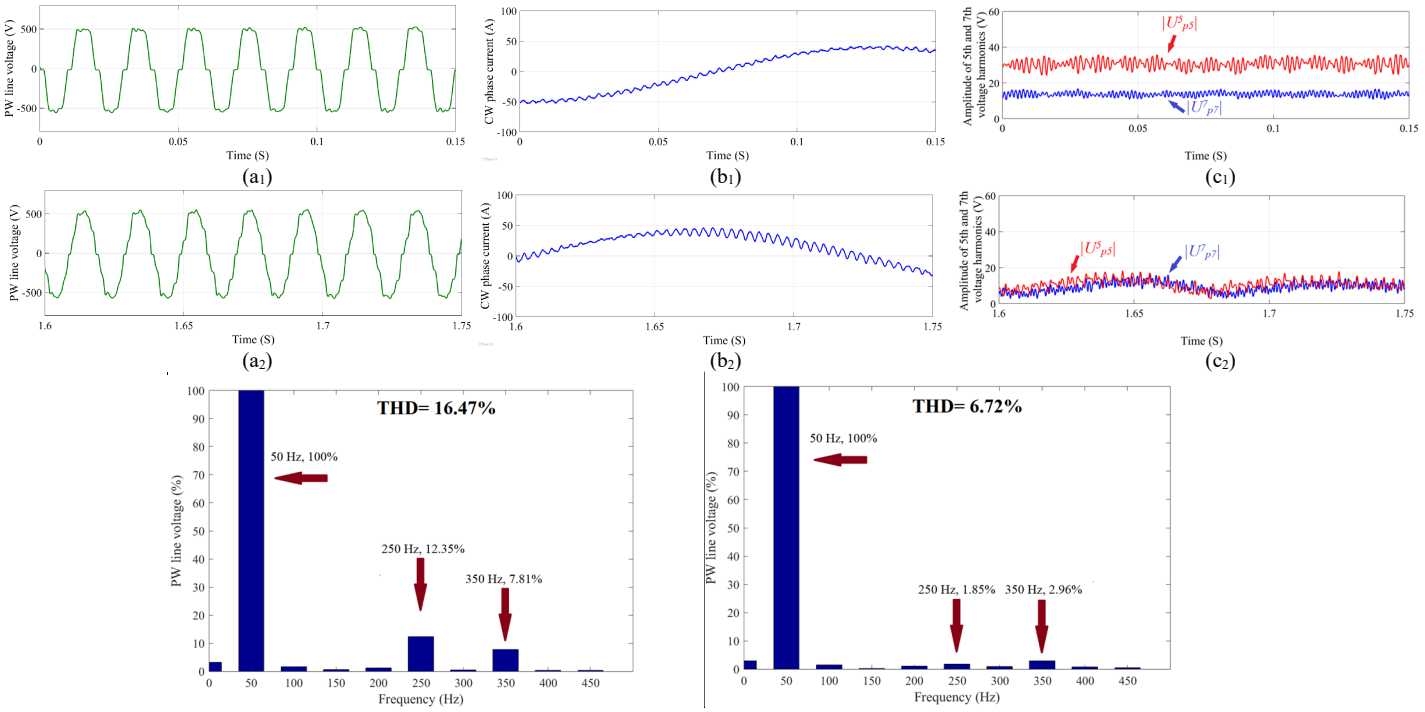

Fig. 11. Experimental results using nonlinear load at 675 rpm (subscripts 1and 2 represent the conventional and proposed strategy respectively). (a) PW voltage. (b) CW current. (c) PW phase voltage amplitude in 5th and 7th harmonics. (d) THD of PW voltage.

sinusoidal. The THD of PW voltage is reduced from 12.12% to 4.7% as shown in Fig. 13(g), and the amplitude of negative sequence component is reduced from around 17 V to 5 V.

E. Results Under Unbalanced Nonlinear Load

In this experiment, the BDFIG works under unbalanced nonlinear load, this situation is realized via adopting a single-phase diode rectifier with a resistor of 25 Ω at the dc side with the reference value of PW voltage 173V. From Fig. 14, the BDFIG starts to work under the proposed strategy. The amplitude of the negative sequence component reaches around 35 V, and the THD of the PW line voltage reaches 2.11%. From 3.05 s, the system works under the conventional strategy. The amplitude of the negative sequence component increases immediately to around 80 V, and the THD of the PW line voltage reaches to 6.43%.

VII. Conclusion

In general, the standalone BDFIG is sensitive to unusual load conditions. The unbalanced and nonlinear loads can cause significant unbalance and distortion for PW voltage. To overcome of this issue, the DRC-based control method in MSC is proposed to compensate the unbalanced and distorted PW voltage at the same time. In comparison with the previous methods, the proposed method is without any filter for extracting the negative-sequence and harmonic components, and can significantly reduce the numbers of PIR, P and PI controllers to enhance the system response. In addition, the design methodology of the DRC is easier and the computational burden can be decreased. Satisfactory simulation and

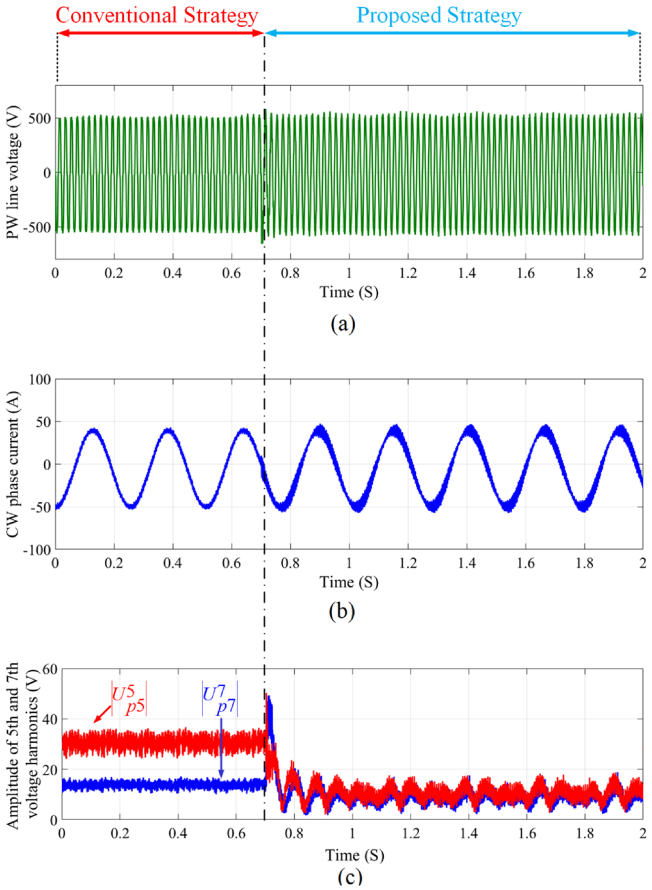

Fig. 12. Measured dynamics with nonlinear load at 675 rpm. (a) PW voltage. (b) CW current. (c) PW phase voltage amplitude in 5th and 7th harmonics.

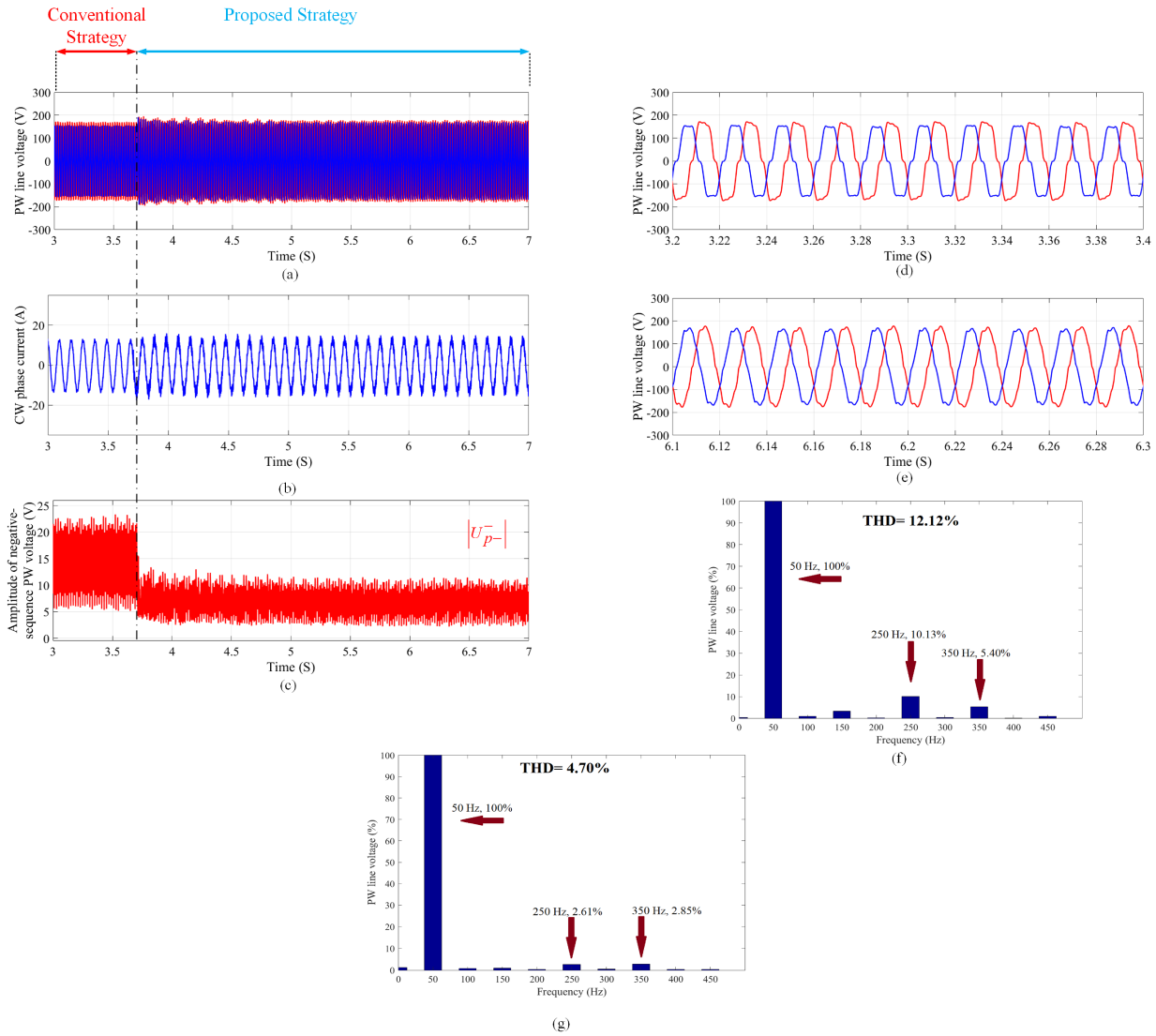

Fig. 13. Experimental results with unbalanced and nonlinear loads. (a) PW line voltage. (b) CW phase current. (c) Amplitude of negative-sequence PW voltage. (d) Extended scenery of (a). (e) Extended scenery of (a). (f) THD and harmonic spectrum of the PW voltage shown in (d). (g) THD and harmonic spectrum of the PW voltage shown in (e).

experiments can be achieved when the BDFIG in the standalone mode works under four kinds of typical loads (i.e., unbalanced load, nonlinear load, unbalanced and nonlinear loads, and unbalanced nonlinear load), which verifies the effectiveness of the proposed method.

REFERENCES

[1] S. Shao, E. Abdi, F. Barati, and R. McMahon, “Stator-flux-oriented vector control for brushless doubly-fed induction generator,” *IEEE Trans. Ind. Electron.*, vol. 56, no. 10, pp. 4220-4228, Oct. 2009.

[2] T. Long, S. Shao, P. Malliband, E. Abdi, and R. A. McMahon, “Crowbarless fault ride-through of the brushless doubly fed induction generator in a wind turbine under symmetrical voltage dips,” *IEEE Trans. Ind. Electron.*, vol. 60, no. 7, pp. 2833-2840, Jul. 2013.

[3] R. Sadeghi, S. M. Madani, M. Ataei, M. R. A. Kashkooli, and S. Ademi, “Super-twisting sliding mode direct power control of a brushless doubly fed induction generator,” *IEEE Trans. Ind. Electron.,* vol. 65, no. 11, pp. 9147-9156, Nov. 2018.

[4] S. Shao, T. Long, E. Abdi, and R. A. McMahon, “Dynamic control of the brushless doubly fed induction generator under unbalanced operation,” *IEEE Trans. Ind. Electron.,* vol. 60, no. 6, pp. 2465-2476, Jun. 2013

[5] T. Long, S. Shao, E. Abdi, R. A. McMahon, and S. Liu, “Asymmetrical low-voltage ride through of brushless doubly fed induction generators for the wind power generation,” *IEEE Trans. Energy Convers.,* vol. 28, no. 3, pp. 502-511, Sep. 2013.

[6] J. Chen, W. Zhang, B. Chen, and Y. Ma, “Improved vector control of brushless doubly fed induction generator under unbalanced grid conditions for offshore wind power generation,” *IEEE Trans. Energy Convers.,* vol. 31, no. 1, pp. 293-302, Mar. 2016.

[7] T. Wu, X. Wang, and Y. Li, "The scalar control research based on fuzzy PID of BDFM stand-alone power generation system." *in Proc. Int. Conf. Electr. Inf. Control Eng.*, 2011, pp. 2806-2809.

[8] Y. Liu, W. Ai, B. Chen, K. Chen, and G. Luo, “Control design and experimental verification of the brushless doubly-fed machine for stand-alone power generation applications,” *IET Elect. Power Appl.,* vol. 10, no. 1, pp. 25-35, Jan. 2016.

[9] L. Sun, Y. Chen, L. Peng, and Y. Kang, “Numerical-based frequency domain controller design for stand-alone brushless doubly fed induction generator power system,” *IET Power Electron.,* vol. 10, no. 5, pp. 588-598, Feb. 2017.

[10] L. Sun, Y. Chen, J. Su, D. Zhang, L. Peng, and Y. Kang, “Decoupling network design for inner current loops of stand-alone brushless doubly fed induction generation power system,” *IEEE Trans. Power Electron.*, vol. 33, no. 2, pp. 957-963, Feb. 2018.

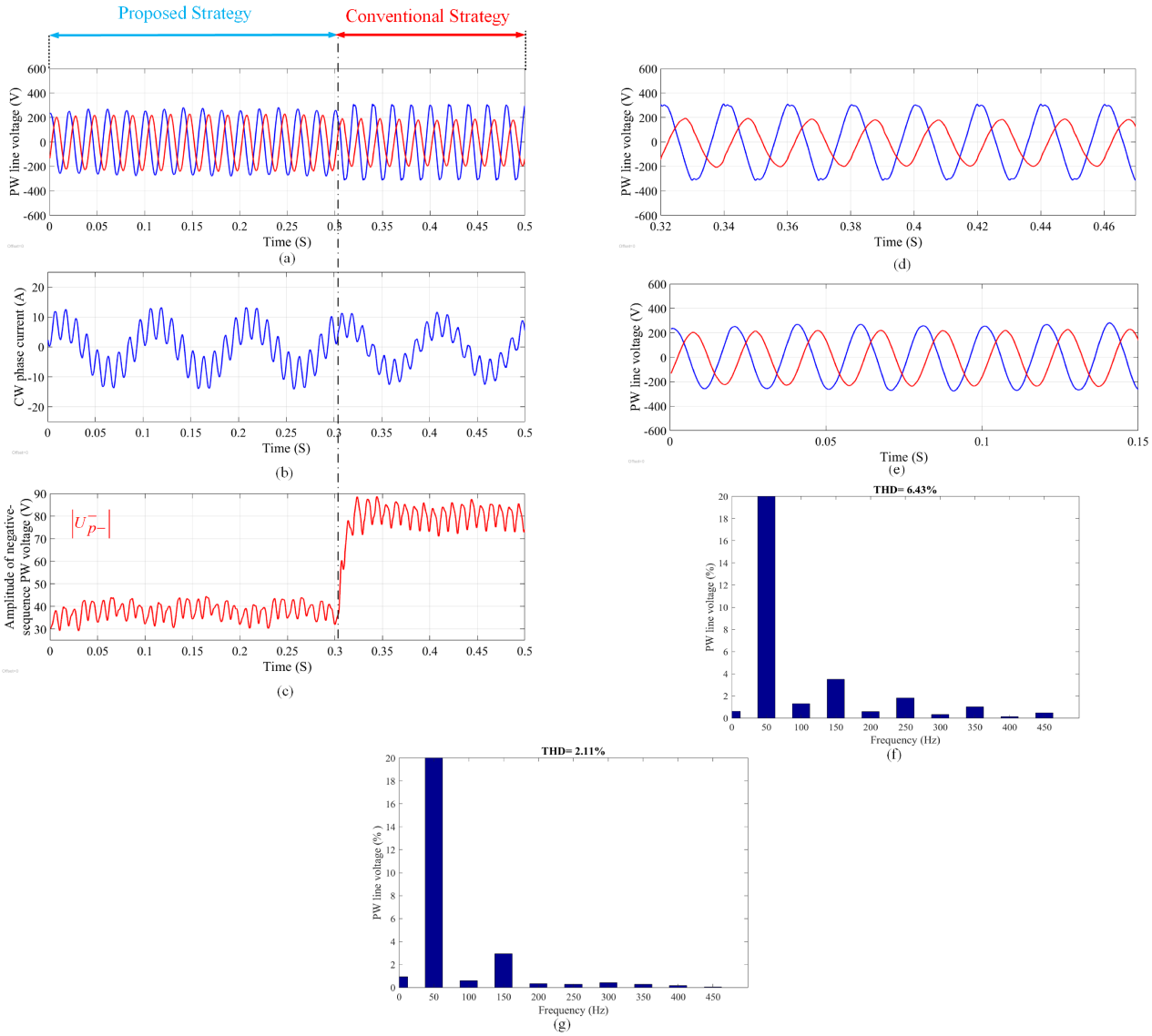

Fig. 14. Experimental results with unbalanced nonlinear load. (a) PW line voltage. (b) CW phase current. (c) Amplitude of negative-sequence PW voltage. (d) Extended scenery of (a). (e) Extended scenery of (a). (f) THD and harmonic spectrum of the PW voltage shown in (d). (g) THD and harmonic spectrum of the PW voltage shown in (e).

[11] A. B. Ataji, Y. Miura, T. Ise, and H. Tanaka, "Direct voltage control with slip angle estimation to extend the range of supported asymmetric loads for stand-alone DFIG," *IEEE Trans. Power Electron.*, vol. 31, no. 2, pp. 1015-1025, Feb. 2016.

[12] F. Wei, X. Zhang, D. M. Vilathgamuwa, S. S. Choi, and S. Wang, "Mitigation of distorted and unbalanced stator voltage of stand-alone doubly fed induction generators using repetitive control technique," *IET Elect. Power Appl.*, vol. 7, no. 8, pp. 654-663, Sep. 2013.

[13] R. Pena, R. Cardenas, E. Escobar, J. Clare, and P. Wheeler, "Control system for unbalanced operation of stand-alone doubly fed induction generators," *IEEE Trans. Energy Convers.,* vol. 22, no. 2, pp. 544-545, Jun. 2007.

[14] Y. Liu, W. Xu, J. Zhu, and F. Blaabjerg, "Sensorless control of standalone brushless doubly-fed induction generator feeding unbalanced loads in ship shaft power generation system," *IEEE Trans. Ind. Electron.*, vol. 66, no. 1, pp. 739-749, Jan. 2019.

[15] W. Xu, O. M. E. Mohammed, Y. Liu, and M. R. Islam, "Negative sequence voltage compensating for unbalanced standalone brushless doubly-fed induction generator," *IEEE Trans. Power Electron.*, vol. 35, no. 1, pp. 667-680, Jan. 2020.

[16] W. Xu, D. Dong, Y. Liu, K. Yu, and J. Gao, "Improved sensorless phase control of stand-alone brushless doubly-fed machine under unbalanced loads for ship shaft power generation," *IEEE Trans. Energy Convers.*, vol. 33, no. 4, pp. 2229-2239, Dec. 2018.

[17] W. Xu, K. Yu, Y. Liu, and J. Gao, "Improved coordinated control of standalone brushless doubly-fed induction generator supplying nonlinear loads," *IEEE Trans. Ind. Electron.*, vol. 66, no.11, pp. 8382-8393, Nov. 2019.

[18] R. A. McMahon, P. C. Roberts, X. Wang, and P. J. Tavner, "Performance of BDFM as generator and motor," *IEE Proc. Electr. Power Appl.,* vol. 153, no. 2, pp. 289-299, Mar. 2006.

[19] V. Phan and H. Lee, "Control strategy for harmonic elimination in stand-alone DFIG applications with nonlinear loads," *IEEE Trans. Power Electron*., vol. 26, no. 9, pp. 2662-2675, Sep. 2011.

[20] J. F. Eggleston, "Harmonic modelling of transmission systems containing synchronous machines and static convertors," PhD thesis, University of Canterbury, 1985.

[21] Z. Lu, H. Yang, and A. J. Zhang, "New magnetic integration of full-wave rectifier with center-tapped transformer," *International Power Electronics and Application Conference and Exposition*, 2014, pp. 609-613.

[22] X. Wei, M. Cheng, W. Wang, P. Han, and R. Luo, "Direct voltage control of dual-stator brushless doubly fed induction generator for stand-alone wind energy conversion systems," *IEEE Trans. Magn.,* vol. 52, no. 7, pp. 1-4, Jul. 2016.

Omer Mohammed Elbabo Mohammed received the B.Sc. degree from the University of Kordofan, EL-Obied, Sudan, in 2010, and the M.Sc. degree from the Sudan University of Science and Technology, Khartoum, Sudan, in 2013, all in electrical engineering. Since September 2016, he has been working toward the Ph.D. degree with the State Key Laboratory of Advanced Electromagnetic Engineering and Technology, School of Electrical and Electronic Engineering, Huazhong University of Science and Technology, Wuhan, China. He was a Lecturer with the Department of Electrical Engineering, Faculty of Engineering, University of Sinnar, Sinnar, Sudan, in 2013. His current research interests include ac electrical machine control and power quality issues.

Wei Xu (M'09-SM'13) received the double B.E. and M.E. degrees from Tianjin University, Tianjin, China, in 2002 and 2005, and the Ph.D. from the Institute of Electrical Engineering, Chinese Academy of Sciences, in 2008, respectively, all in electrical engineering. His research topics mainly cover design and control of linear/rotary machines.

From 2008 to 2012, he made Postdoctoral Fellow with University of Technology Sydney, Vice Chancellor Research Fellow with Royal Melbourne Institute of Technology, Japan Science Promotion Society Invitation Fellow with Meiji University, respectively. Since 2013, he has been full professor with State Key Laboratory of advanced Electromagnetic Engineering in Huazhong university of Science and Technology, China. He has more than 100 papers accepted or published in IEEE Transactions Journals, two edited books published by Springer Press, one monograph published by China Machine Press, and 120 Invention Patents granted or pending, all in the related fields of electrical machines and drives. He is Fellow of the Institute of Engineering and Technology (IET). He will serve as the General Chair for 2021 International Symposium on Linear Drives for Industry Applications (LDIA 2021) and 2023 IEEE International Conference on Predictive Control of Electrical Drives and Power Electronics (PRECEDE 2023), in Wuhan, China, respectively. He has served as Associate Editor for several leading International Journals, such as IEEE Transactions on Industrial Electronics, and so on.

Yi Liu (M'14) received his B.E. and M.E. degrees in Automation and Control Engineering from the Wuhan University of Science and Technology, Wuhan, China, in 2004 and 2007, respectively; and his Ph.D. degree in Mechatronic Engineering from the Huazhong University of Science and Technology, Wuhan, China, in 2016.

From March 2016 to June 2016, he was a Senior R & D Engineer at the Fourth Academy of China Aerospace Science and Industry Group, Wuhan, China. From July 2016 to October 2019, he was a Postdoctoral Research Fellow at the State Key Laboratory of Advanced Electromagnetic Engineering and Technology, Huazhong University of Science and Technology, where he has been a Lecturer since January 2020. He is the Vice Chair for IEEE IES Wuhan Chapter. His current research interests include multi-port electrical machines and drive systems.

Frede Blaabjerg (S'86–M'88–SM'97–F'03) was with ABB-Scandia, Randers, Denmark, from 1987 to 1988. From 1988 to 1992, he got the PhD degree in Electrical Engineering at Aalborg University in 1995. He became an Assistant Professor in 1992, an Associate Professor in 1996, and a Full Professor of power electronics and drives in 1998. From 2017 he became a Villum Investigator. He is honoris causa at University Politehnica Timisoara (UPT), Romania and Tallinn Technical University (TTU) in Estonia.

His current research interests include power electronics and its applications such as in wind turbines, PV systems, reliability, harmonics and adjustable speed drives. He has published more than 600 journal papers in the fields of power electronics and its applications. He is the co-author of four monographs and editor of ten books in power electronics and its applications.

He has received 32 IEEE Prize Paper Awards, the IEEE PELS Distinguished Service Award in 2009, the EPE-PEMC Council Award in 2010, the IEEE William E. Newell Power Electronics Award 2014, the Villum Kann Rasmussen Research Award 2014, the Global Energy Prize in 2019, and the 2020 IEEE Edison Medal. He was the Editor-in-Chief of the IEEE Transactions on Power Electronics from 2006 to 2012. He has been Distinguished Lecturer for the IEEE Power Electronics Society from 2005 to 2007 and for the IEEE Industry Applications Society from 2010 to 2011 as well as 2017 to 2018. In 2019-2020 he serves a President of IEEE Power Electronics Society. He is Vice-President of the Danish Academy of Technical Sciences too. He is nominated in 2014-2019 by Thomson Reuters to be between the most 250 cited researchers in Engineering in the world.